Nano Today 53 (2023) 102025

Contents lists available at ScienceDirect

Nano Today

journal homepage: www.elsevier.com/locate/nanotoday

Bimodal single-atom iron nanozyme biosensor for volatile amine and food freshness detection

Guangchun Song [a,b,1], Zedong Zhang [c,1], Marie-Laure Fauconnier [b], Cheng Li [a], Li Chen [a], Xiaochun Zheng [a,*], Dequan Zhang [a,*]

[a] Institute of Food Science and Technology, Chinese Academy of Agricultural Sciences, Key Laboratory of Agro-products Quality and Safety Control in Storage and Transport Process, Ministry of Agriculture and Rural Affairs, Beijing 100193, China
[b] Laboratory of Chemistry of Natural Molecules, Gembloux Agro-Bio Tech, University of Liege, Passage des déportés 2, B-5030 Gembloux, Belgium
[c] Department of Chemistry, Tsinghua University, Beijing 100084, China

ARTICLE INFO

Keywords:
Single-atom iron nanozyme
Peroxide-like enzymes
Freshness
Dual-signal biosensor
Food safety

ABSTRACT

Volatile amines (VAs) play a critical role in detecting the freshness of meat. However, the development of nondestructive, real-time, and portable techniques for monitoring VAs remains a challenge. Here, we successfully created a colorimetric-fluorescent dual-signal biosensor for meat freshness detection by using a single-atom iron nanozyme (SAFe-N-C nanozyme) and carbon quantum dots (CDs). The SAFe-N-C nanozyme with high peroxidase-like (POD-like) activity (40.22 U/mg) acts as a catalyst by facilitating the conversion of the colourless reduced state 3,3′,5,5′-tetramethylbenzidine ($_{red}$TMB) to its oxidized product ($_{ox}$TMB). Subsequently, the fluorescence signal of the CDs is quenched due to the inner filtering effect (IFE) between $_{ox}$TMB and CDs. During food spoilage, the generation of VAs results in the reduction of $_{ox}$TMB, which subsequently recovers the fluorescence of the CDs. As a result, the limits of detection (LOD) for ammonia detection are 0.9840 ppm and 0.0838 ppm within a linear range of 0.5–50 ppm. This colorimetric-fluorescent dual-signal biosensor effectively detects VAs during the spoilage of livestock and poultry meat in a nondestructive and real-time manner. This innovative work overcomes the limitation of single signal output and provides a portable and reliable method for VAs detection, proving to be a significant advancement in meat freshness assessment.

Introduction

Food is prone to contamination by external and internal microorganisms throughout various stages, including processing, transportation, storage, and marketing. These microorganisms can decompose proteins to produce volatile amines (VAs), leading to the deterioration of food [1]. Since the 1970 s, VAs have been recognized as indicators of food spoilage and deterioration in the food industry, significantly influencing the evaluation of food flavour and quality [2]. Moreover, VAs have adverse effects on human health, including symptoms such as loss of appetite, headache, nausea, vomiting, and other related ailments [3]. While methods such as gas chromatography [4,5], gas mass spectrometry [6,7], and high-performance liquid chromatography [8] have been employed for VAs detection, they have certain limitations, such as the need for professional operation and high cost. Consequently, there is a growing need to develop real-time, cost-effective, and efficient methods for monitoring VAs to ensure food quality and safety.

Recently, single-atom nanozymes (SAzymes) with exceptional catalytic performance have found extensive applications in biomedicine [9–13], environmental detection [14], and food authentication [15,16], which is primarily due to their ability to generate synergistic colorimetric, fluorescent, and/or electrochemical signal outputs. However, most of these nanozymes are designed to respond to a single-signal, making their results vulnerable to interference from external environmental factors, which exhibit inadequate sensitivity and low accuracy [17–20]. The utilization of multisignal sensing systems offers numerous advantages, including enhanced sensitivity, strong selectivity, reduced time consumption, and portability [21,22]. Despite these benefits, there have been limited studies focusing on constructing multisignal for VAs assays based on the catalytic activity of SAzymes. The exploration of multisignal VAs assays could potentially revolutionize VAs detection

* Corresponding authors.
E-mail addresses: zhengxiaochun321@163.com (X. Zheng), dequan_zhang0118@126.com (D. Zhang).
[1] These authors contributed equally to this work.

https://doi.org/10.1016/j.nantod.2023.102025
Received 3 July 2023; Received in revised form 25 September 2023; Accepted 8 October 2023
Available online 14 October 2023

and improve overall food safety measures. Carbon quantum dots (CDs) are specific fluorescent nanomaterials derived from carbon sources with good solubility, biocompatibility, and low toxicity [23–25]. The green fluorescent CDs used in our study decreases the interference of background fluorescence, making the detection results more reliable. Given the outstanding physicochemical attributes of CDs and the remarkable enzymatic catalytic properties of SAzymes, the development of a portable, rapid, and efficient multisignal biosensor system for VAs detection makes it highly promising for applications in the field of food safety.

In this study, a novel and efficient colorimetric-fluorescent dual-signal biosensor for detecting VAs was developed. The biosensor was prepared by physically combining a single-atom iron nanozyme (SAFe-N-C nanozyme) with CDs (Scheme 1). Under pH range of 2–4, the SAFe-N-C nanozyme efficiently catalyses the colourless reduced state 3,3′,5,5′-tetramethylbenzidine ($_{red}$TMB) into its oxidized products ($_{ox}$TMB), which displayed a UV–vis absorption peak at 652 nm. However, the emission fluorescence of CDs at 475 nm is quenched due to the inner filtering effect (IFE) arising from the interaction between $_{ox}$TMB and CDs [26–29]. The content of the intermediate hydroxyl radical (•OH) in the system decreased with increasing pH value, which subsequently led to a decrease in $_{ox}$TMB content. Thus, the fluorescence of the CDs gradually recovered as the IFE weakened. In this way, the biosensor enabled the quantitative determination of VAs through a colorimetric-fluorescent dual-signal approach within the same detection system.

Experimental section

Materials

Zinc nitrate hexahydrate ($Zn(NO_3)_2{\cdot}6H_2O$, analytical grade, 98%, Bei Jing tongguang fine chemicals), iron acetylacetonate (III) ($Fe(acac)_3$, analytical grade, 99%, China National Pharmaceutical Group Co., Ltd.), 2-methylimidazole (analytical grade, 98%, Alfa Aesar), N,N-dimethylformamide (analytical grade, Sinopharm Chemical), methanol (analytical grade, Sinopharm Chemical), and triethylamine (analytical grade, Acros Organics) were used without any further purification. 3,3′,5,5′-Tetramethylbenzidine (TMB) was purchased from Shanghai McLean Biochemical Technology Co., Ltd. Carbon quantum dots (CDs) were purchased from Beijing Jinruilin Technology Development Co., LTD. Whatman No. 1 filter paper was purchased from Shanghai Jinpan Biotechnology Co., Ltd. Sodium acetate (NaHAc) and absolute ethanol (C_2H_5OH) were purchased from Shanghai Yuanye Biotechnology Co., Ltd. Glacial acetic acid (HAc). Natural orseradish peroxidase was purchased from Beijing Hedder Technology Co. Pork, beef, lamb, and chicken were all purchased from local supermarkets.

Synthesis of SAFe-N-C nanozyme

To prepare SAFe-N-C nanozyme, 1.190 g of $Zn(NO_3)_2{\cdot}6H_2O$ and 141 mg of iron acetylacetonate (III) were dissolved in 20 mL of methanol and sonicated to prepare solution A. Solution B was obtained by dissolving 1.314 g of 2-methylimidazole in 15 mL of methanol. Solution B was mixed with solution A and stirred for 10 mins. Furthermore, the mixed solution was transferred to a 50 mL Teflon reactor and heated at 120 ℃ for 4 h in a constant temperature oven. The orange precipitate was collected by centrifugation, washed six times with N,N-dimethylformamide and twice with methanol until the supernatant appeared colourless and transparent and then dried at 80 ℃. The SAFe-N-C nanozyme was produced by calcining the orange precipitate above at 950 ℃ for 3 h under flowing nitrogen gas with a heating rate of 5 ℃ min^{-1}.

Characterization of the SAFe-N-C nanozyme

Transmission electron microscope (TEM) images of catalysts were collected with a Hitachi H-800 TEM. High angle annular dark field scanning TEM (HAADF-STEM) images were recorded by a JEOL JEM-2100 F with an electron acceleration energy of 200 kV, which was equipped with a probe spherical aberration corrector. X-ray powder diffraction (XRD) spectra were obtained by using a Rigaku RU-200b X-ray diffractometer equipped with Cu K_α radiation ($\lambda = 1.5406$ Å). X-ray photoelectron spectroscopy (XPS) spectra were collected with ULVAC PHI Quantera. The X-ray absorption find structure (XAFS) spectra were taken at the 1W1B station in the Beijing Synchrotron Radiation Facility (BSRF, operated at 3.5 GeV with a maximum current of 250 mA, Fe K-edge under fluorescence excitation mode). The XAFS data of the Fe foil and Fe_2O_3 reference were used as references and measured in transmission mode using an ionization chamber. The XAFS data of the SAFe-N-C nanozyme was collected at room temperature in fluorescence excitation mode using a Lytle detector and Mn filter.

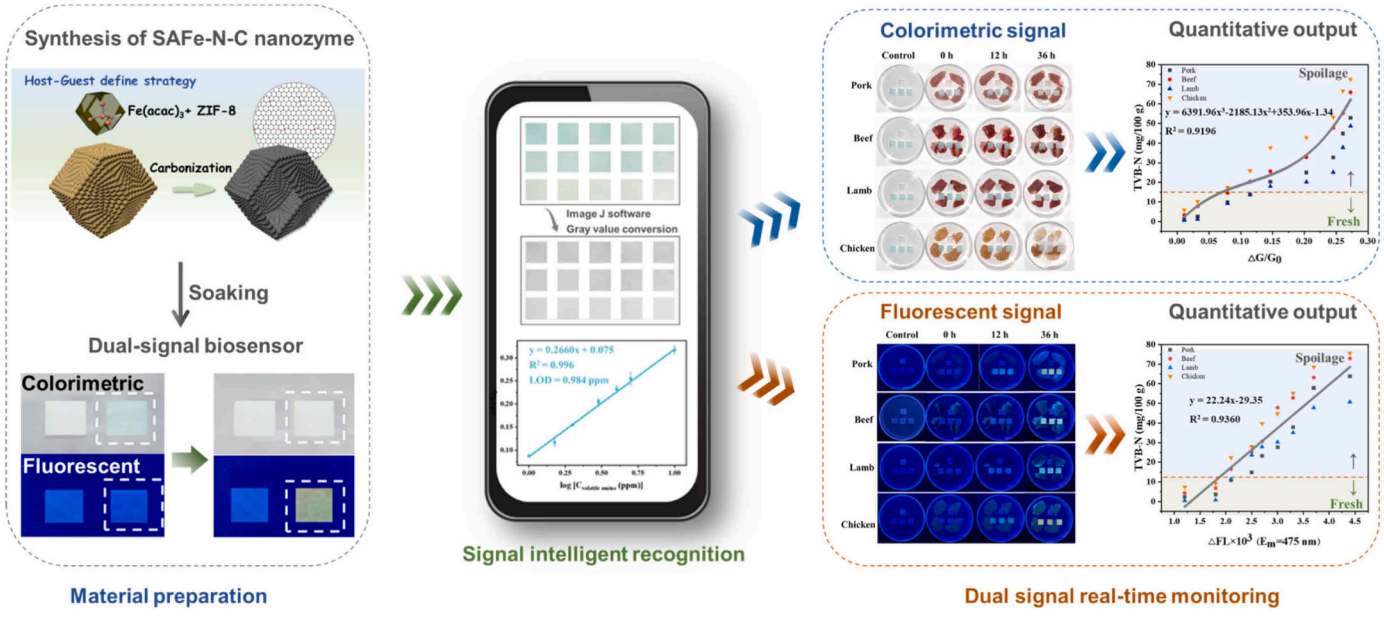

Scheme 1. Portable visualization of a colorimetric-fluorescent dual-signal biosensor for detection applications.

Preparation of the SAFe-N-C nanozyme solution

The synthesized SAFe-N-C nanozyme was dissolved in ethanol and ultrasonically dissolved to obtain the SAFe-N-C nanozyme stock solution (90 μM) for future use.

Preparation of the CDs solution

The CDs stock solution was prepared in anhydrous ethanol at a concentration of 1.0 mg/mL and stored in the dark for future use.

Verification of POD-like catalytic activity

170 μL of acetic acid buffer solution with a pH value of 4.0, 20 μL of TMB solution (20 mM), and 10 μL of H_2O_2 solution (9.8 M) were mixed evenly in a 96-well plate, and then 10 μL of SAFe-N-C nanozyme solution was added and incubated for 10 mins. The colour change of the system and the UV–vis absorption peak at 652 nm were recorded. The SAFe-N-C nanozyme shows POD-like activity when the colour of the solution changes to blue and a UV–vis absorption peak appears at 652 nm.

Optimization of POD-like reaction conditions

We observed SAFe-N-C nanozyme and natural horseradish peroxidase at different pH values (pH 2, 4, 6, 8, and 12), catalytic reaction times (0, 0.5, 1, 3, 5, 7, 9, and 11 mins), and temperatures (−18, 4, 25, 37, 45, and 55 ℃), recording the UV–vis absorption peak changes at 652 nm.

Calculation of POD-like catalytic activity parameters

Under the optimum reaction conditions, different concentrations of TMB (0.025, 0.05, 0.1, 0.2, 0.4, 0.8, 1.6, 3.2, 6.4, 12.8, and 25.6 mM) and SAFe-N-C nanozyme (0.9, 1.8, 2.7, 3.6, 4.5, 5.4, 6.3, 7.2, and 8.1 μM) were recorded at 10 s intervals over 400 s. The data were further fitted by the Michaelis-Menten equation to calculate the typical parameters of enzyme-like activity, including the Michaelis constant (K_m), maximal reaction velocity (v_{max}), catalytic constant (K_{cat}), and single atom nanozyme enzyme-like activity (SA) parameter values.

Preparation of the colorimetric-fluorescent paper detection sensor

Firstly, Whatman No. 1 filter paper was cut into 2 × 2 cm paper sheets. After soaking them in SAFe-N-C nanozyme solution and CDs solution for 30 mins, and we processed the bioactive paper at 37 ℃ for approximately 15 mins until the paper dried. Finally, the resulting dried paper-base was the colorimetric-fluorescent dual-signal biosensor.

Optimization of the colorimetric-fluorescent dual-signal biosensor system conditions

The changes in the UV–vis absorbance peak at 652 nm and the fluorescence emission intensity at 475 nm were recorded by varying the concentration of substrate (0.5, 1.0, 1.5, and 2.0 mM), reaction time (5, 10, 15, 20, and 25 min) and SAFe-N-C nanozyme concentration (1.8, 5.4, 9.0, 12.6, and 16.2 μM).

Determination of the limit of detection (LOD)

The LOD was determined based on the 3σ method.

$$LOD = 3\ \sigma/k$$

where σ was the standard deviation of the blank (20 samples) and k was the slope between plotting the grey value (or the fluorescent intensity) versus VAs content.

Reusability testing

After the colorimetric-fluorescent dual-signal biosensor was used for the detection of ammonia, it was placed in hydrochloric acid solution (0.1 M) and incubated for 20 mins. Then, it was subjected to cyclic operation, and the reproducibility experiment was determined by measuring the relative activity of the colorimetric-fluorescent dual-signal biosensor.

Validity testing

Accelerated experiments were performed at ambient temperatures of 40, 45, 50, 55, and 60 °C using a 4 °C storage environment as a control, and the validity of the colorimetric-fluorescent dual-signal biosensor at 25 °C was calculated by the Arrhenius equation.

Monitoring the freshness of meat samples

Livestock meat (pork, beef, and lamb) and poultry meat (chicken) samples were collected for practical monitoring. Both the samples and colorimetric-fluorescent dual-signal biosensor were placed at 25 °C for monitoring in a sealed petri dish without contact. The changes in visible colour and fluorescence were recorded by a smartphone and fluorescence spectrometer, respectively. The quantitative and discriminative detection of the colorimetric-fluorescent dual-signal biosensor system were achieved by grey value (ImageJ software) and fluorescence intensity detection. For comparison, the freshness in four kinds of samples during storage was verified by TVB-N according to the national standard method of P.R. China (GB 5009.228–2016 and GB 2707–2016).

Results and discussion

Structural characterization of SAFe-N-C nanozyme

The SAFe-N-C nanozyme was prepared through host-guest define strategy (Fig. 1a). $Fe(acac)_3$ was confined in the multistage pore structure of ZIF-8, which inhibited the agglomeration of Fe elements to form iron nanoparticles during further calcination. The orthododecahedral morphology was preserved after calcination, and the size of the carbon carrier was approximately 400 nm (Fig. 1b). $Fe(acac)_3$ will provide Fe atoms and form stable Fe-N_4 coordination above the N-doped C skeleton. In the magnified AC-HAADF-STEM image, the bright spots marked with higher contrast represent single Fe atoms that were uniformly dispersed on the carbon support (Fig. 1c). The mass content of Fe in the material was quantified by ICP-OES as 1.8 wt%. In the XRD pattern, the SAFe-N-C nanozyme only contained a broad peak at 19° and 38°, indicating the presence of amorphous carbon (Fig. S1, Supporting Information). There were no Fe nanoparticles in the material. Furthermore, we characterized the coordination environment of the SAFe-N-C nanozyme by XPS. Characterization by XPS proved the existence of pyrrolic and pyridinic N, which provide sufficient sites for Fe centre coordination (Fig. S2, Supporting Information). Both XPS and XANES spectra showed that the oxidation state of Fe element is between +2 and +3 (Fig. 1d). By performing K^2 weighting treatment on the data in the EXAFS region, we can obtain K-space curves (Fig. S3, Supporting Information). The SAFe-N-C nanozyme and phthalocyanine Fe (FePc) showed nearly consistent peak shapes in the low K range, indicating that the SAFe-N-C nanozyme has a similar coordination environment in the first shell as FePc. Furthermore, we performed Fourier transform (FT) EXAFS on the structure to obtain R-space curves (Fig. 1e). We can obtain the first shell peak at 1.49 Å corresponding to the Fe-N path. There is no peak at 2.2 Å, which corresponds to the Fe-Fe path in SAFe-N-C (all peak positions without phase transfer). The fitting result of the R-space curve verifies that the SAFe-N-C nanozyme has Fe-N_4 coordination in the first shell (Fig. 1f, Fig. S4, and

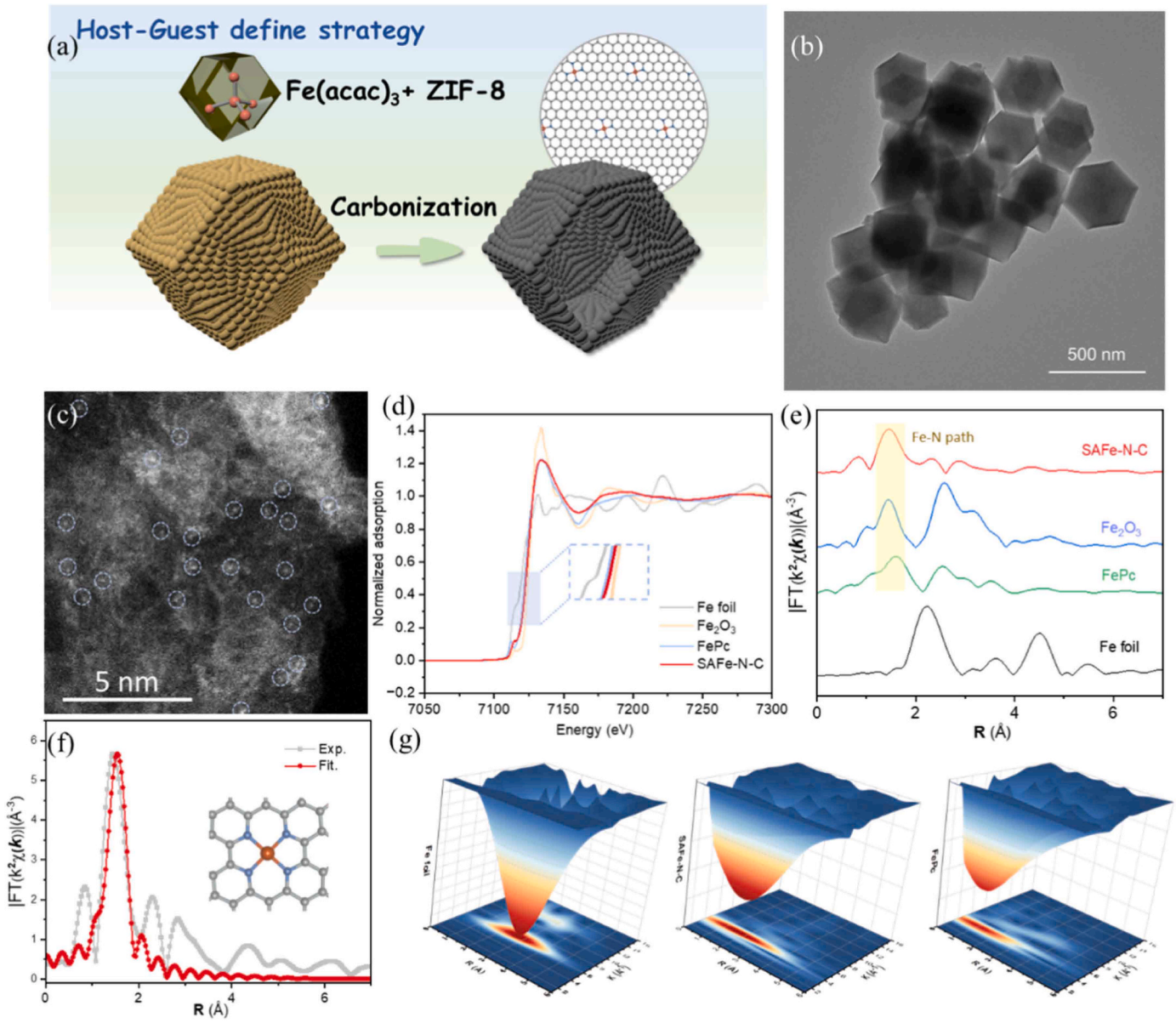

Fig. 1. Characterization of SAFe-N-C nanozyme. a) Schematic diagram of the SAFe-N-C nanozyme synthesis. b) TEM image of SAFe-N-C nanozyme. c) Magnified AC-HAADF-STEM image of the SAFe-N-C nanozyme. d) XANES spectra of Fe foil, SAFe-N-C nanozyme, Fe_2O_3, and FePc K edge. e) R-space spectra of SAFe-N-C nanozyme and references. f) The fitting result of the SAFe-N-C nanozyme. g) 3D colour map WT-XAFS images of different Fe references.

Table S1, Supporting Information). By wavelet transform (WT-XAFS), we can more clearly see some possible peaks hidden in the background signal-to-noise ratio. In Fig. 1g, the peak positions of the SAFe-N-C nanozyme and FePc are almost completely consistent, and the peak region of Fe foil (Fe-Fe path) does not exist in SAFe-N-C nanozyme and FePc.

Mimicking POD-like catalytic property of SAFe-N-C nanozyme

TMB is often used as an effective substrate to explore the POD-like catalytic performance of SAFe-N-C nanozyme [30] (Fig. 2a). When TMB, H_2O_2, and SAFe-N-C nanozyme form a mixture system, an obvious colour change and a UV–vis absorption peak at 652 nm can be observed (Fig. 2a, b). This phenomenon can be ascribed to the SAFe-N-C nanozyme, which can catalyse H_2O_2 to produce •OH and oxidize the colourless $_{red}$TMB substrate to blue $_{ox}$TMB. ESR was used to analyse the catalytic process to reveal the catalytic mechanism of the SAFe-N-C nanozyme. The •OH signals (capture agent DMPO) can be observed in Fig. 2c, indicating the formation of •OH during the reaction. As verified, the SAFe-N-C nanozyme showed similar optimal conditions of pH value and reaction time, with a wider temperature tolerance range, compared to natural enzymes (Fig. S5a, b, c, Supporting Information). Under optimal catalytic reaction conditions, the catalytic performance of different Fe-based nanozymes was further analyzed [16,31,32], as shown in Table S2. The lower K_m value of 0.30 mM and higher SA value of 40.22 U/mg, compared with natural horseradish peroxidase and other SAzymes, indicated that the SAFe-N-C nanozyme had a very strong POD-like catalytic activity (Fig. 2d, e, Table S2, Supporting Information).

Colorimetric-fluorescent dual-signal biosensor mechanism

It is well known that the pH of the system has an important effect on the catalytic reaction of SAzymes, which can affect their surface charge transfer and the content of intermediates, thus affecting the catalytic rate [32–34]. VAs generated from food spoilage have the capability to

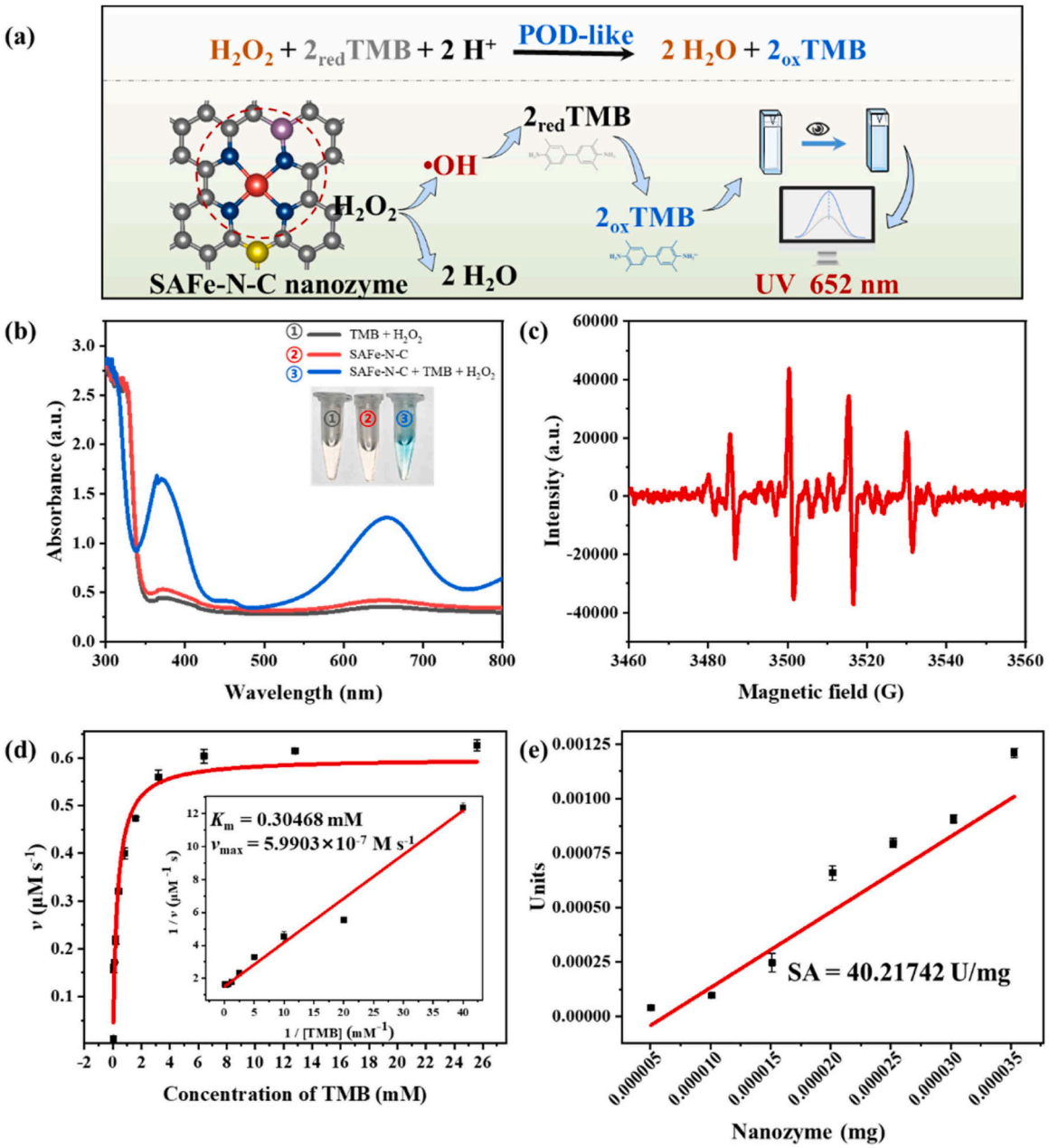

Fig. 2. POD-like catalytic performance of the SAFe-N-C nanozyme. a) UV–vis absorption spectra of different systems at 300–800 nm. b) Electron spin resonance (ESR). c) Michaelis-Menten equation (the illustration is Lineweaver-Burk). d) SAFe-N-C nanozyme enzyme-like activity.

upregulate the pH value in the optimal POD-like catalytic system of SAFe-N-C nanozyme and further affects the content of the intermediate •OH to reduce the production of $_{ox}$TMB. Thereafter, the IFE between $_{ox}$TMB and CDs was alleviated, and the fluorescent emission of CDs recovered gradually. In this way, a colorimetric-fluorescent dual-signal biosensor system was constructed for the detection of VAs (Fig. 3a).

To verify the colorimetric-fluorescent dual-signal sensing mechanism, the experiments were conducted in two independent systems, colorimetric and fluorescent modes, to investigate the interference between the components. The UV–vis absorption peak at 652 nm only appeared when SAFe-N-C nanozyme, $_{red}$TMB, and H_2O_2 simultaneously existed, and the production of $_{ox}$TMB could not be affected by CDs (Fig. S6a, Supporting Information). The fluorescence of CDs showed good stability within 90 mins (Fig. S7a, Supporting Information) and was completely quenched after mixing SAFe-N-C nanozyme, $_{red}$TMB, H_2O_2, and CDs for 15 mins (Fig. S6b, 7b, Supporting Information). The content of the intermediate product •OH was examined after the system reacted for 10 mins to obtain reliable data. The UV–vis absorption peak at 652 nm sequentially decreased and disappeared for the systems spiked with 10 ppm and 50 ppm ammonia (Fig. 3b), while the content of •OH in the corresponding systems was significantly reduced (Fig. 3c). The results verified that the existence of VAs decreased the content of intermediate •OH, thus reducing the formation of $_{ox}$TMB, alleviating IFE and restoring the fluorescence of CDs.

Sensor performance of the dual-signal biosensor for ammonia

Some key parameters, such as substrate addition, reaction time, and enzyme addition of the colorimetric-fluorescent dual-signal biosensor system, were further optimized, and the results are shown in Fig. S8. Based on the optimal parameters of the system, SAFe-N-C nanozyme, $_{red}$TMB, H_2O_2, and CDs components were loaded on Whatman No. 1

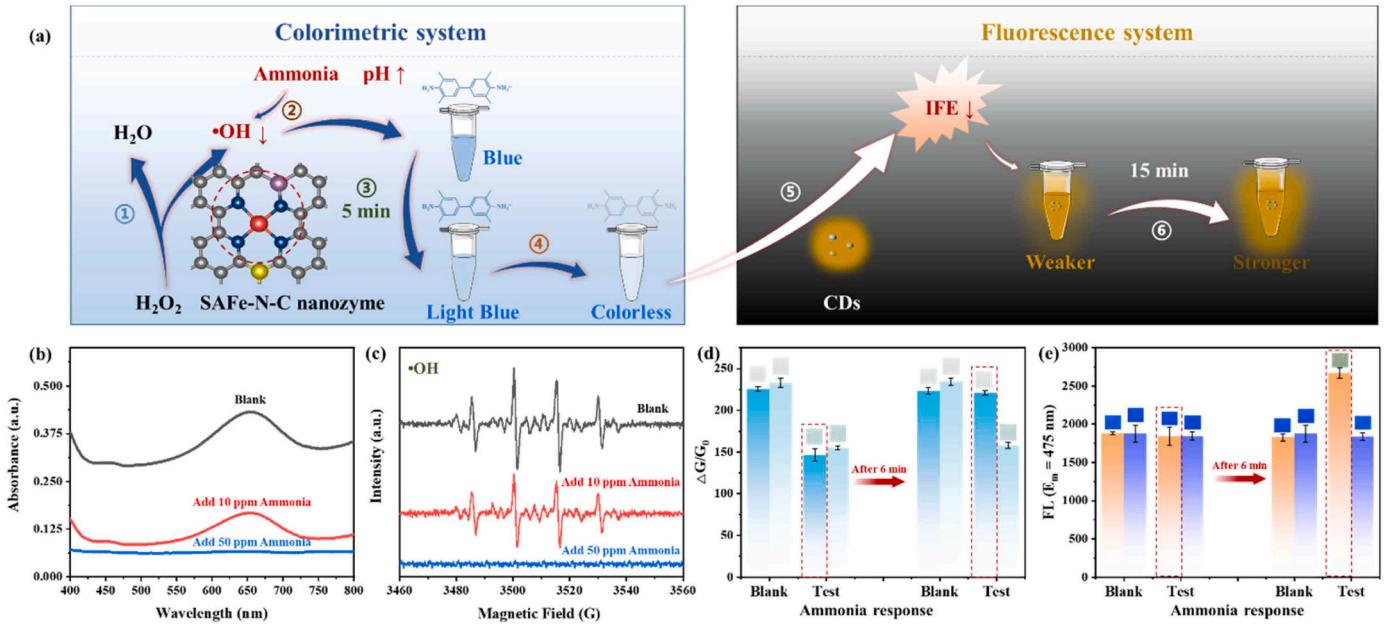

Fig. 3. Detection mechanism of the colorimetric-fluorescent dual-signal biosensor. a) Diagram of the dual-signal biosensor. b) Scans of UV–vis absorption peak of different systems in the range of 400–800 nm. c) Detection of •OH in different systems. d) Visible response of dual-signal biosensor to 10 ppm ammonia. e) Fluorescence response of the dual-signal biosensor to 10 ppm ammonia.

paper-based carriers to construct a portable colorimetric-fluorescent dual-signal biosensor for VAs detection. A model reactor was developed with a colorimetric-fluorescent dual-signal biosensor, 10 ppm ammonia, and a petri dish, as shown in Fig. S9a. The colour of the colorimetric-fluorescent dual-signal biosensor changed from blue to colourless after 6 mins, while no obvious colour change occurred in the control group (Fig. 3d, Fig. S9a, Supporting Information). The fluorescence of the dual-signal biosensor was clearly observed to change from blue to yellow-green fluorescence upon excitation at 365 nm (Fig. 3e, Fig. S9b, Supporting Information). In addition, the colorimetric-fluorescent dual-signal biosensor had good stability when stored at 25 °C (Fig. S10a, Supporting Information) and was valid for three years (Fig. S10b, Supporting Information). It can be reused four times or more, and its performance was much better than that of natural horseradish peroxidase (one more) (Fig. S10c, Supporting Information). All the above results proved that the colorimetric-fluorescent dual-signal biosensor has good stability, reusability, and higher economic benefits.

Visual quantification of ammonia

The response time (t_{90}) and LOD are important parameters of a sensor, which gives an idea about the effectiveness of applications. The response time and sensitivity of the colorimetric-fluorescent dual-signal biosensor were investigated in an ammonia system at 0.5–50 ppm. The t_{90} was confirmed as 6 mins when the colour of the colorimetric-fluorescent dual-signal biosensor changed from blue to colourless (Fig. 4a, Fig. S11, Supporting Information). The LOD was calculated as 0.9840 ppm in the linear range of 1.5–10 ppm (Fig. 4b), which showed a reliable detection performance of the dual-signal biosensor compared with previous studies (Table S3, Supporting Information). After excitation at 365 nm, the colour of the colorimetric-fluorescent dual-signal biosensor changed from blue to yellow-green (Fig. 4c), and the t_{90} was 15 mins (Fig. 4d, e). In the linear range of 10–30 ppm, the LOD was 0.0838 ppm (Fig. 4f), which also indicated a reliable detection performance (Table S3, Supporting Information).

Qualitatively and quantitatively monitoring the freshness of meat samples

The colorimetric-fluorescent dual-signal biosensor was used to monitor freshness changes of pork, beef, lamb, and chicken at 25 ℃ without damaging the sample (Fig. S12, Supporting Information). As shown in Fig. 5a and Fig. S12, visible and fluorescent colour photographs of the colorimetric-fluorescent dual-signal biosensor during the storage period of 42 h were recorded. The spoilage times of pork beef, lamb, and chicken were 30 h, 24 h, 36 h, and 12 h, respectively. The visible and fluorescent colours of the control group did not change until the end of storage. The grey value and fluorescence intensity values of the colorimetric-fluorescent dual-signal sensor were quantified and displayed in Fig. 5b, c (Table S4 and S5, Supporting Information). The total volatile basic nitrogen (TVB-N) value was measured to monitor freshness changes in meat with a limit of $\leq$ 15 mg/100 g for raw meat according to national standard methods (GB 5009.228–2016, GB 2707–2016). It was observed that the values of TVB-N in pork, beef, lamb, and chicken increased from 0.92, 2.23, 0.031, and 4.37 mg/100 g to 52.8, 65.9, 48.7, and 72.6 mg/100 g, respectively, with storage from 0 h to 42 h. Furthermore, quantitative models between the grey value, fluorescence intensity of colorimetric-fluorescent the dual-signal sensor and TVB-N value of the meat samples were built as shown in Fig. 5d, e (Fig. S13, Table S6, Supporting Information). The correlation coefficients were 0.9196 and 0.9360, respectively. Therefore, the colorimetric-fluorescent dual-signal biosensor developed in this study had reliability in the process of practical sample testing compared to previous assays (Table S3).

Conclusion

In summary, a colorimetric-fluorescent dual-signal biosensor was successfully constructed for food freshness detection by synergistically coordinating SAFe-N-C nanozyme with CDs. The colorimetric absorption peak at 652 nm was induced by the catalysis of SAFe-N-C nanozyme to change $_{red}$TMB to $_{ox}$TMB, followed by the emission fluorescence of CDs at 475 nm which was quenched due to the IFE arising from the interaction between $_{ox}$TMB and CDs. The combined characteristics were utilized to provide a real-time and precise detection method for the fresh

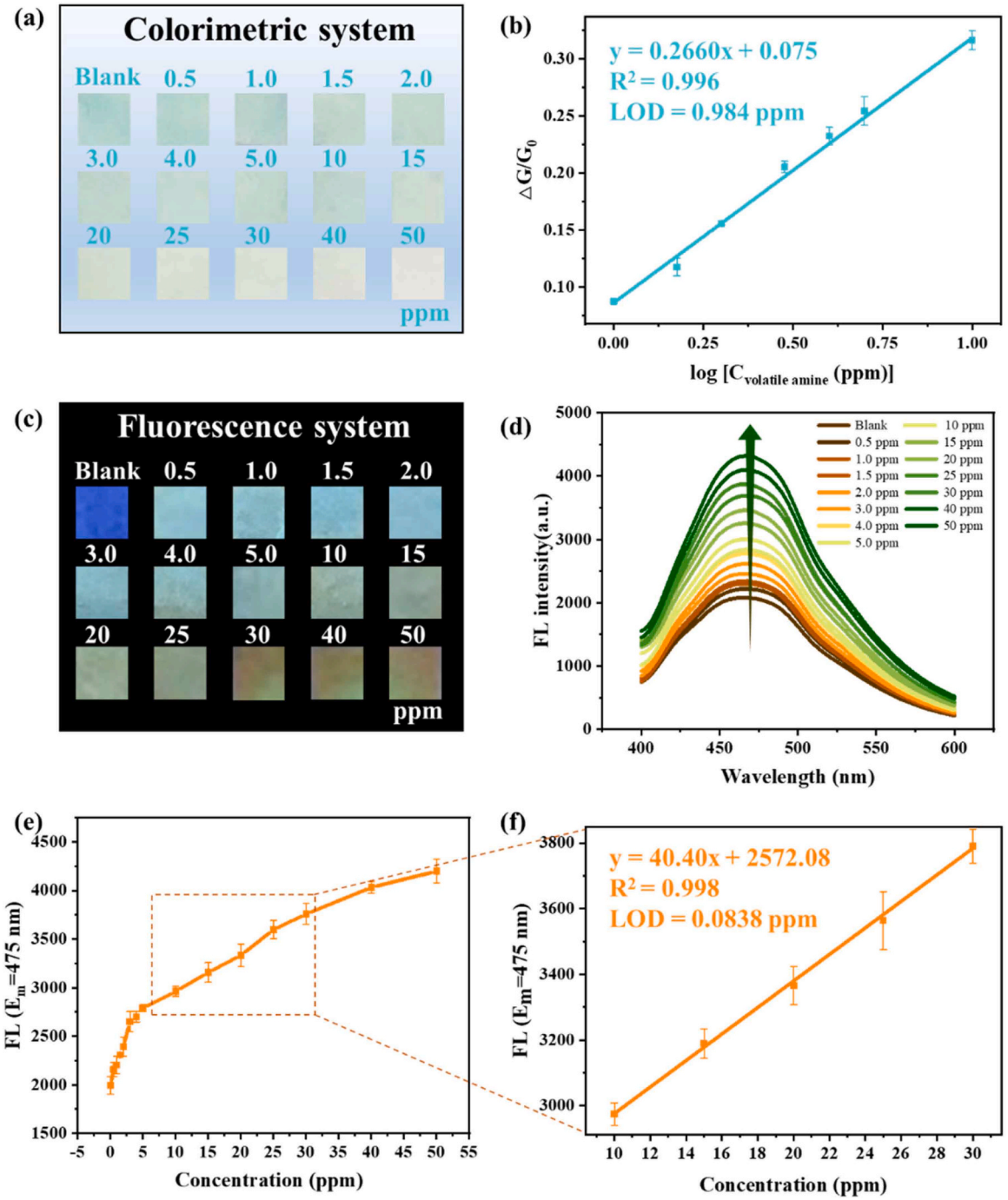

Fig. 4. Sensitivity of the colorimetric-fluorescent dual-signal biosensor. a) Visible response of the dual-signal biosensor to different concentrations of ammonia. b) Linear correlation between the grey values and the concentration of ammonia. c) Fluorescence response of the dual-signal biosensor to different concentrations of ammonia. d) Fluorescence spectral response of the dual-signal biosensor to different concentrations of ammonia. e) Correspondence between 475 nm fluorescence intensity in d) and the concentration of ammonia f) Linear correlation between fluorescence intensity and the concentration of ammonia.

detection of food. The response times are 6 mins and 15 mins, respectively, when exposed to volatile alkaline gases such as ammonia, trimethylamine, and cadaverine for colorimetric mode and fluorescent mode, respectively. The LOD values for these two modes were 0.9840 ppm and 0.0838 ppm, respectively. The developed dual-signal sensor shows some advantages in accuracy and anti-interference. This dual-signal sensor could obtain optical signals rapidly by a portable phone-based program, which is suitable for monitoring the volatile alkaline gases in meat. In other words, this study provides a design strategy for constructing a portable, accurate, and rapid multisignal detection method for detecting the freshness of food.

CRediT authorship contribution statement

Guangchun Song: Methodology, Investigation, Formal analysis, Data curation, Writing – original draft. **Zedong Zhang:** Methodology, Investigation, Software, Formal analysis, Writing – review & editing. **Marie-Laure Fauconnier:** Investigation, Formal analysis. **Cheng Li:** Writing – review & editing. **Li Chen:** Conceptualization, Supervision, Writing – review & editing. **Xiaochun Zheng:** Conceptualization,

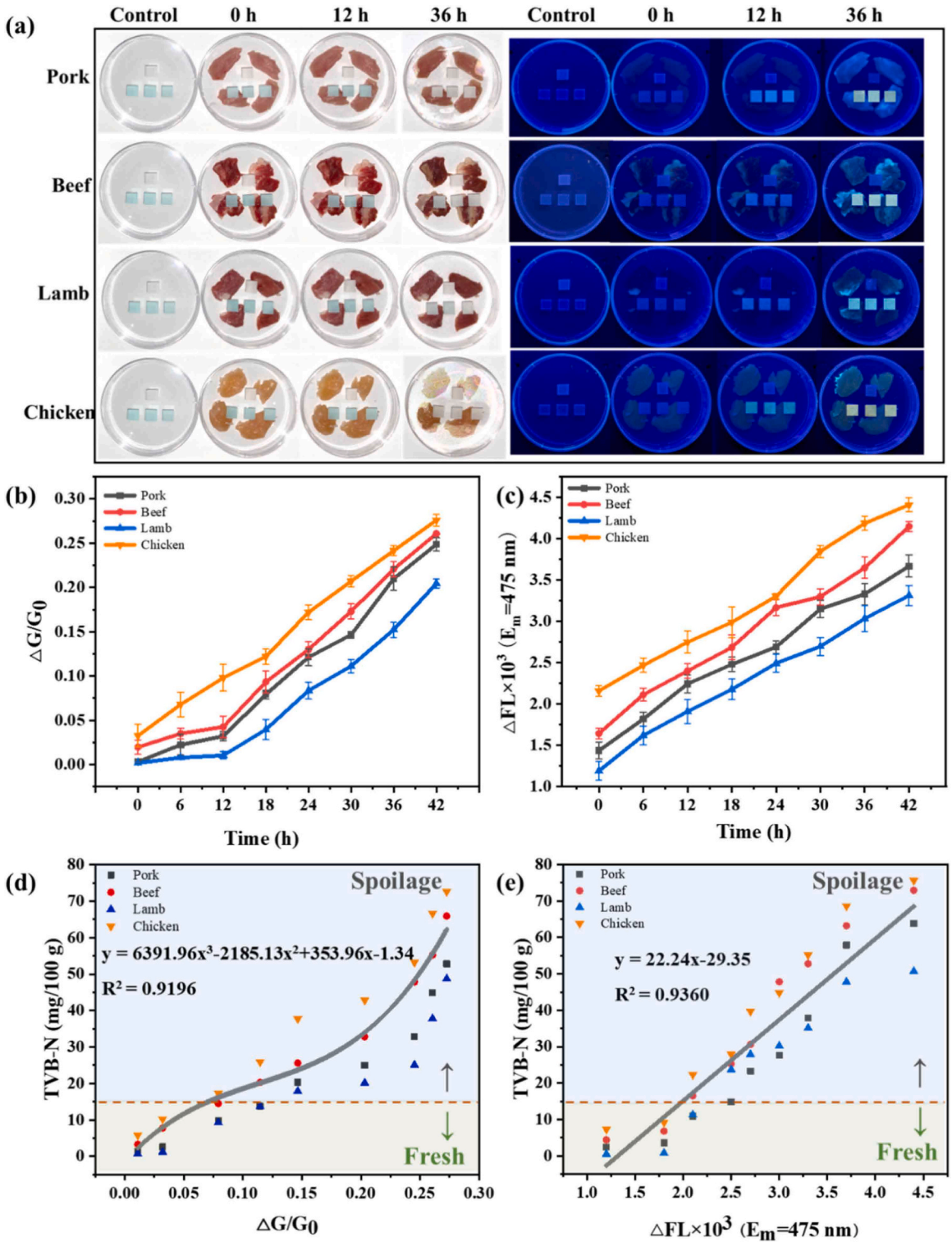

Fig. 5. Practical sample freshness detection. a) Colorimetric-fluorescent dual-signal biosensor monitoring the freshness of pork, beef, lamb, and chicken stored at 25 °C with visual colorimetric and fluorescent colour. b) Relationship between colorimetric-fluorescent dual-signal biosensor grey value ($\Delta G/G_0$) and storage time in pork, beef, lamb, and chicken. c) Relationship between colorimetric-fluorescent dual-signal biosensor fluorescence values (ΔFL) and TVB-N values in pork, beef, lamb, and chicken. d) Relationship between colorimetric-fluorescent dual-signal biosensor grey values and storage time in pork, beef, lamb, and chicken. e) Relationship between colorimetric-fluorescent dual-signal biosensor fluorescence values and TVB-N values in pork, beef, lamb, and chicken.

Supervision, Validation, Writing – review & editing. **Dequan Zhang:** Supervision, Validation, Writing – review & editing, Funding acquisition.

Declaration of Competing Interest

The authors declare that they have no known competing financial interests or personal relationships that could have appeared to influence the work reported in this paper.

Data availability

Data will be made available on request.

Acknowledgements

This work was financially supported by the National Key R&D Program of China (2022YFD2100500).

Supporting Information

Supporting Information is available from the author.

Appendix A. Supporting information

Supplementary data associated with this article can be found in the online version at doi:10.1016/j.nantod.2023.102025.

References

[1] J. Chen, X. Zhang, A.P. Bassey, X. Xu, F. Gao, K. Guo, G. Zhou, Crit. Rev. Food Sci. Nutr. 14 (2022) 1–21.
[2] L. Sun, A. Rotaru, Y. Garcia, J. Hazard. Mater. 437 (2022) 129364–129378.
[3] M. Ma, S. Xu, Q. Liu, J. Xu, Y. Li, Environ. Sci. Technol. 56 (2022) 16189–16199.
[4] K. Ueta, Chromatographia 82 (2019) 317–323.
[5] G.C. Graffius, B.M. Jocher, D. Zewge, H.M. Halsey, G. Lee, F. Bernardoni, X. Bu, R. Hartman, E.L. Regalado, J. Chromatogr. A 1518 (2017) 70–77.
[6] L. Lacalle-Bergeron, T. Portolés, C. Sales, M. Carmen Corell, F. Domínguez, J. Beltrán, J. Vicente Sancho, F. Hernández, Food Res. Int. 137 (2020) 109698–109707.
[7] B.E. Vitova, Chem. Pap. 74 (2020) 1679–1690.
[8] I.C. Chao, C.M. Wang, S.P. Li, L.G. Lin, Molecules 23 (2018) 1568–1577.
[9] C. Peng, R. Pang, J. Li, E. Wang, Adv. Mater. 7 (2023) e2211724–e2211830.
[10] B. Jiang, Z. Guo, M. Liang, Nano Res. 16 (2023) 1878–1889.
[11] D.B. Cheng, G.B. Qi, J.Q. Wang, Y. Cong, F.H. Liu, H. Yu, Z.Y. Qiao, H. Wang, Biomacromolecules 18 (2017) 1249–1258.
[12] D.B. Cheng, X.H. Zhang, S.Y. Chen, X.X. Xu, H. Wang, Z.Y. Qiao, Adv. Mater. 34 (2022) 2109528–2109536.
[13] D.Y. Hou, N.Y. Zhang, M.D. Wang, S.X. Xu, Z.J. Wang, X.J. Hu, G.T. Lv, J.Q. Wang, X.H. Wu, L. Wang, Angew. Chem. Int. Ed. 61 (2022) 202116893–202116903.
[14] V. Kandathil, S.A. Patil, Adv. Colloid Interface Sci. 294 (2021) 102485–102499.
[15] G. Song, J.C. Li, Z. Majid, W. Xu, X. He, Z. Yao, Y. Luo, K. Huang, N. Cheng, Food Chem. 390 (2022) 133127–133134.
[16] G. Song, J. Zhang, H. Huang, X. Wang, X. He, Y. Luo, J.C. Li, K. Huang, N. Cheng, Food Chem. 387 (2022) 132896–132905.
[17] X. Jiang, H. Jin, Y. Sun, R. Gui, Microchim. Acta 186 (2019) 580–592.
[18] X. Bu, Y. Fu, X. Jiang, H. Jin, R. Gui, Microchim. Acta 187 (2020) 154–164.
[19] M. Wang, R. Shi, M. Gao, K. Zhang, L. Deng, Q. Fu, L. Wang, D. Gao, Food Chem. 318 (2020) 126506–126517.
[20] Rijun Gui, Xiangning Bu, Weijie He, Hui Jin, New J. Chem. 42 (2018) 16217–16225.
[21] J.J. Hu, W. Jiang, Q. Chen, R. Liu, X. Lou, F. Xia, Anal. Chem. 93 (2021) 14036–14041.
[22] A. Lc, L.A. Lu, W.A. Dong, A. Xt, B. Dx, A. Ll, Y.A. Chao, A. Yn, Sens. Actuators B: Chem. 303 (2020) 127277–127286.
[23] L. Tian, Z. Li, P. Wang, X. Zhai, X. Wang, T. Li, J. Energy Chem. 55 (2021) 279–294.
[24] Y. Liu, H. Huang, W. Cao, B. Mao, Y. Liu, Z. Kang, Mater. Chem. Front. 4 (2020) 1586–1613.
[25] A. Xu, G. Wang, Y. Li, H. Dong, S. Yang, P. He, G. Ding, Small 16 (2020) 2004621–2004652.
[26] X. Li, S. Ding, Z. Lyu, P. Tieu, M. Wang, Z. Feng, X. Pan, Y. Zhou, X. Niu, D. Du, W. Zhu, Y. Lin, Small 18 (2022) 2203001–2203011.
[27] Shujuan Zhuo, Zhang Changqing, Shen Ping, Weili, Anal. Methods 11 (2019) 2663–2668.
[28] P. Ni, C. Chen, Y. Jiang, C. Zhang, Y. Lu, Sens. Actuators B Chem. 301 (2019) 127080–127087.
[29] P. Fan, C. Liu, C. Hu, F. Li, X. Lin, S. Yang, F. Xiao, New J. Chem. 46 (2022) 2526–2533.
[30] L. Huang, J. Chen, L. Gan, Sci. Adv. 5 (2019) 5490–5499.
[31] J. Bing, D. Demin, G. Lizeng, Z. Mengjie, F. Kelong, T. Yan, X. Juqun, B. Yuhai, T. Zhou, G.G. Fu, Nat. Protoc. 13 (2018) 1506–1520.
[32] G. Song, J. Xu, H. Zhong, Q. Zhang, X. Wang, Y. Lin, S.P. Beckman, Y. Luo, X. He, J. C. Li, K. Huang, N. Cheng, Research 6 (2023) 0095–0106.
[33] N. Cheng, J.C. Li, D. Liu, Y. Lin, Small 15 (2019) 1901485–1901492.
[34] R.Z. Juqun Xi, Liming Wang, Wei Xu, Qian Liang, Jingyun Li, Jian Jiang, Yili Yang, Xiyun Yan, Kelong Fan, Lizeng Gao, Adv. Funct. Mater. 31 (2020) 2007130–2007144.